SCIENTIFIC
REPORTS

natureresearch

OPEN

Nitrogen-based gas molecule adsorption of monolayer phosphorene under metal functionalization

Shuangying Lei, Ran Gao, Xiaolong Sun, Sijia Guo, Hong Yu, Neng Wan, Feng Xu & Jie Chen

Using the first-principles calculation based on density functional theory (DFT), the adsorption properties of nitrogen-based gases molecules (NH_3, NO, NO_2) on various metal (Li, Na, K, Rb, Cs, Ca, Sr, Ba, Ni, La, Tl) decorated phosphorene systems have been studied systematically. The results show that all metal decorations can improve the adsorption strength of phosphorene to nitrogen-based gases molecules except for Tl decoration. Especially, the adsorption energy of NH_3 molecule on Ni decorated phosphorene is 1.305 eV, and the adsorption energies of NO and NO_2 on La decorated phosphorene can be up to 2.475 and 3.734 eV, respectively. In addition, after NO and NO_2 adsorptions, the electronic and magnetic properties of some metal decorated phosphorenes change, indicating that the metal decorated phosphorenes have great potential in NO and NO_2 detection.

Nowadays, many human activities, such as burning, motor vehicle exhaust, and chemical production processes, produce polluting gases. Among many atmospheric pollutants, nitrogen-based gases (NO, NO_2, NH_3) have received widespread attention in recent years due to their threat to the ecological environment (acid rain, ozone depletion, photochemical smog) and human health[1–5]. Thus, the removal and detection of nitrogen-based exhaust gases from environment is essential. Traditionally, metal oxide semiconductors have been widely used to detect of nitrogen-based gases due to low cost, low power consumption and simplicity in measurements[6–9]. However, their long recovery period and low specificity limit the application in high measurement accuracy gas detection[10].

The emergence of nanotechnology, especially the successful stripping of graphene[11,12], opens up new avenues for gas detection. The large surface-to-volume ratio makes it be a good candidate for gas detection and removal[13–15]. The excellent gas detection capabilities of graphene were demonstrated, and the results showed that the sensitivity can reach a single gas molecule[16]. However, theoretical studies found that the interaction between pristine graphene and small molecule gases is rather weak[17], and the adsorption strength of gas molecules can be improved by introducing decoration or doping atoms into graphene[18,19]. Recently, another single element 2D material, phosphorene, was successfully obtained by mechanical stripping methods. Unlike C atoms with inherent inertness, the chemically active of the phosphorus atom makes the phosphorene have stronger interaction with the atoms or molecules than graphene[20–24]. Especially for gas molecules, the studies indicate that phosphorene has the potential to compete with or even exceed graphene in gas adsorption and detection[22,23]. For example, Mayorga-Martinez *et al.* studied the sensing of methanol molecules based on a two-dimensional phosphorene sensor, and the results showed that the sensitivity can reach 28 ppm[25]. The experimental results by Abbas *et al.* showed that the detection sensitivity of NO_2 down to 5 ppb[26]. Furthermore, the puckered honeycomb structure of phosphorene provides more adsorption space for adsorbate than the planar structure of graphene. Based on surface adsorption, the researchers studied the application of phosphorene in Na^+ and Li^+ batteries, and the results showed that the capacity found to be ~400 and ~700 mAhg^{-1} for Na and Li batteries[27–30], respectively. Additionally, other applications based on surface decoration, such as hydrogen storage[31,32] and the removal of polluting gases[33–35], have been extensively theoretically investigated, and the results showed that the decoration of atoms can greatly improve the adsorption capacity and strength of phosphorene to the gas molecules.

In this paper, the behavior of nitrogen-based gas molecules adsorption on pristine and various metal (Li, Na, K, Rb, Cs, Ca, Sr, Ba, Ni, La, Tl) decorated phosphorene were studied systematically. It is found that all metal decorations can improve the adsorption strength of nitrogen-based gas molecules on phosphorene, except for

Key Laboratory of Microelectro mechanical Systems of the Ministry of Education, Southeast University, Nanjing, 210096, China. Correspondence and requests for materials should be addressed to S.L. (email: lsy@seu.edu.cn)

1

NO molecule on Tl decorated phosphorene, and thus metal decorated phosphorenes have great potential for application in nitrogen-based gas removal. Furthermore, the electrical and magnetic properties of some metal decorated phosphorene have interesting change after NO and NO_2 adsorption, indicating that metal decorated phosphorenes have great potential in NO and NO_2 detection.

Computational Methods

All the density functional theory (DFT) calculation have been implemented by using the Vienna ab initio simulation package (VASP)[36,37]. The generalized gradient approximation (GGA) with the parametrization of Perdew-Burke-Ernzerhof (PBE) was adopted[38]. The empirical correction scheme of Grimme (DFT + D2) was included to correct the effective van der Waals (vdW) interaction[39]. The kinetic energy cutoff was set to be 500 eV for all calculations. The $3 \times 3 \times 1$ mesh grid was sampled in 1st Brillouin zone by using Monkhorst-Pack scheme. To avoid the interaction between periodic adsorbates, the 3×4 supercells were employed. A vacuum of 15 Å was used perpendicular to the phosphorene layer to ensure that the adjacent phosphorene sheets do not interact with each other. For structural optimization, the force convergence criterion on each atom in the structure is less than 0.01 eV/Å. The adsorption energies (E_{ads}) of nitrogen-based gas molecules on pristine phosphorene (bP) and metal decorated phosphorene (bP-M) are calculated by

$$E_{ads} = E_{total} - (E_{bP/bP-M} + E_{adsorbate}) \qquad (1)$$

where E_{total} is the total energy of the adsorption system. E_{bP-M} and Eadsorbate are the energies of bP/bP-M and nitrogen-based gas molecule, respectively.

Results and Discussion

Nitrogen-based gas molecules adsorption on pristine phosphorene. The optimized lattice constants along the armchair and the zigzag direction are 13.722 and 13.225 Å, respectively, and the bandgap is 0.88 eV for 3×4 monolayer phosphorene supercell with 48 phosphorus atoms, which are consistent with the ref.[40]. For the nitrogen-based gas molecules (NH_3, NO, NO_2) on pristine phosphorene, we consider three highly symmetric adsorption sites (hollow, bridge, top, as shown in Fig. 1(a)) and various initial adsorption configurations. After geometry optimization, the most stable adsorption configurations are obtained and shown in Fig. 1(a–c). The nearest atom-to-atom distances between the NH_3, NO and NO_2 molecules and the phosphorenes are 3.192, 2.216 and 2.714 Å, respectively, and the corresponding adsorption energies are 0.212, 0.250 and 0.220 eV. This means the smaller the distances, the larger the adsorption energies. The trend of the distances and adsorption energies are consistent with refs[22,23], and the specific differences between data may be attributed difference exchange-correction functional. The valence radii are 1.07, 0.31, 0.71 and 0.66 for P, H, N and O atoms[21]. The nearest H-P distance of 3.192, N-P distance of 2.216 and O-P distance of 2.714 Å are larger than the sums of corresponding atomic valence radii, indicating that the adsorptions of NH_3, NO and NO_2 on phosphorenes are physical adsorptions. The slices of charge densities in Fig. S5 also corroborate physical adsorption characters. The NO molecule prefers to adsorb on the top site and its N atom point to the surface of phosphorene. The N-O bond length is 1.185 Å, which is slightly larger than that of 1.169 Å for the free NO molecule, due to the interaction between NO molecule and phosphorene. However, the NH_3 and NO_2 molecules prefer to adsorb on the hollow site. To analyze the intrinsic mechanism of the interaction between nitrogen-based gas molecules and phosphorene, the differential charge density (DCD) of the adsorption systems were calculated as shown in Fig. 1(d–f). There is electron transfer between nitrogen-based gas molecules and phosphorene. The charge transfer quantities between the NO/NO_2 molecules and phosphorenes are larger as compared with NH_3 adsorbed case, implying the larger interaction between the NO/NO_2 molecules and phosphorenes and thus larger adsorption energies. The charge transfer quantity between the NH_3 molecule and phosphorene is very small, indicating that the interaction between NH_3 and phosphorene is weak, which is consistent with the minimum adsorption energy. In addition, the Bader charge analysis indicates that the electrons transfer from phosphorene to NO and NO_2 molecules are 0.242 and 0.300 e, respectively, while the electrons transfer from NH_3 molecule to the phosphorene is 0.030 e. Thus, the NO and NO_2 molecules act as acceptors, whereas the NH_3 molecule acts as a donor, which is consistent with ref.[22].

To understand the effects of the adsorption of NO, NO_2 and NH_3 molecules on the electronic properties of phosphorene, the band structures and local density of states (LDOSs) of the adsorption systems were calculated, as shown in Fig. 1(g–l). The adsorption of NO and NO_2 molecules introduce spin polarization in phosphorene, while the NH_3 adsorption system is of zero magnetic moment (see Table 1). In addition, both the conduction band minimum (CBM) and valence band maximum (VBM) for the three adsorption systems remain at the Γ-point. Thus, the adsorption of nitrogen-based gas molecules does not change the direct-bandgap-semiconductor properties of phosphorene, and the corresponding bandgaps are 0.888, 0.869 and 0.899 eV, respectively. For NH_3 adsorbed case, as shown in Fig. 1(j), the states of NH_3 molecule are far from Fermi level, and thus adsorption of NH_3 molecule doesn't change the bandgap of phosphorene. Interestingly, there is a flat band near the Fermi level for the NO and NO_2 molecular adsorption systems, which correspond to the sharp peaks near Fermi level in LDOSs. For NO adsorbed case, strong hybridization of the states between NO molecule and phosphorene near Fermi level is responsible for large interaction and the largest adsorption energy (see Fig. 1(k)). On basis of the definition in ref.[41], the channel of phosphorene with NO adsorption is narrower than that of pristine phosphorene by 0.05 Å, resulting in the stronger repulsive interaction between the facing lone pairs at the ditch, which should be mainly responsible for the decrease of bandgap. For NO_2 adsorbed case, as shown in Fig. 1(l), the coupling peaks near the Fermi levels is mainly arise from NO_2 molecule. Additionally, there are two O peaks near VBM, which is responsible for the large adsorption energy. The charge transfer quantity of 0.3 e from phosphorene to
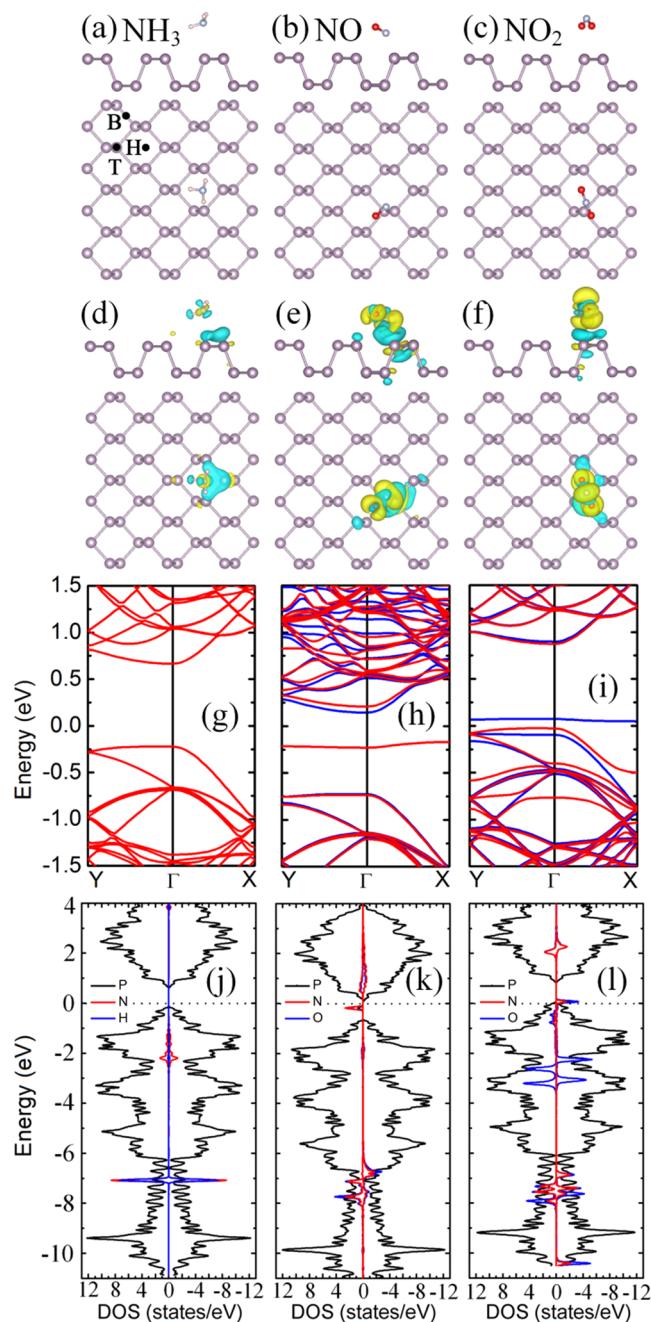
Figure 1. The optimized structure of (**a**) NH$_3$, (**b**) NO and (**c**) NO$_2$ adsorbed on 3 × 4 pristine phosphorene, the corresponding DCD (**d–f**), band structures (**g–i**), and LDOS (**j–l**), respectively. Purple, grey, pink, and red balls in (**a–f**) represent P, N, H and O atoms, respectively. Yellow and blue regions in (**d–f**) denote charge accumulation and charge depletion, respectively. The red and blue curves in (**g–i**) represent the spin-up and spin-down band, respectively. The black, red and blue curves in (**j-l**) represent the LDOS of P, N and H (O), respectively, and the Fermi level is set to zero in (**g–l**).

NO$_2$ molecule reduces the lone pair electrons and thus reduces repulsive interaction between the facing lone pairs at the ditch, which leads to the larger bandgap of 0.899 eV[42].

Metal atoms decorated pristine phosphorene. To further improve the adsorption of phosphorene to nitrogen-based gas molecules, metal atoms are employed to decorate the phosphorene. Considering the growth morphology of metal atom on the surface of the phosphorene, and to avoid the formation of metal clusters, eleven metals with adsorption energy larger than bulk cohesive energy were selected out for decoration aims, namely alkali metal (AM = Li, Na, K, Rb, Cs), alkaline earth metal (AEM = Ca, Sr, Ba), transition metal (TM = Ni, La) and post transition metal (PTM = Tl)[43]. Moreover, the electronic structures of the bP-M systems are shown in Fig. 2 for comparison. Due to the transfer of electrons between the metal atoms and phosphorene, the Fermi

Metal	ΔQ (e)			$D_{\text{P-Gas/M-Gas}}$ (Å)			M (μB)			E_{ads} (ev)		
	NH$_3$	NO	NO$_2$	NH$_3$	NO	NO$_2$	NH$_3$	NO	NO$_2$	NH$_3$	NO	NO$_2$
bP	0.030	−0.242	−0.300	3.192	2.216	2.714	0.000	1.000	0.902	0.212	0.250	0.220
Li	−0.022	−0.466	−0.906	2.012	1.910	1.932	0.000	1.507	0.000	1.079	0.831	2.534
Na	−0.009	−0.398	−0.841	2.404	2.314	2.280	0.000	1.385	0.000	0.821	0.647	2.202
K	0.031	−0.340	−0.708	2.880	2.710	2.647	0.000	1.360	0.166	0.546	0.519	1.823
Rb	0.027	−0.330	−0.692	3.060	2.886	2.791	0.000	1.353	0.192	0.478	0.476	1.738
Cs	0.023	−0.313	−0.664	3.260	3.143	3.010	0.000	1.343	0.240	0.476	0.466	1.705
Ca	0.013	−0.605	−0.802	2.494	2.180	2.310	0.000	1.670	0.000	1.07	1.538	3.485
Sr	−0.005	−0.605	−0.824	2.708	2.348	2.474	0.000	1.679	0.000	0.917	1.363	3.337
Ba	−0.008	−0.569	−0.822	2.841	2.521	2.660	0.000	1.705	0.000	1.066	1.339	3.14
Ni	0.118	−0.332	−0.557	2.034	1.676	1.895	0.000	1.000	1.000	1.305	2.121	1.818
La	0.022	−0.711	−0.770	2.703	2.172	2.469	0.990	0.653	0.000	1.185	2.475	3.734
Tl	0.034	−0.190	−0.717	3.150	2.815	2.575	0.000	1.458	0.000	0.238	0.252	1.773

Table 1. The charge transfer amounts (ΔQ), adsorption distances ($D_{\text{P-Gas/M-Gas}}$) between the nearest P/metal atoms and nitrogen-based gas molecules, magnetic moments (M) and adsorption energies (E_{ads}) for nitrogen-based gas molecules adsorption on pristine/metal decorated phosphorene. Positive ΔQ denotes electron transfer from nitrogen-based gas molecules to pristine/metal decorated substrates.

levels of phosphorene have different degrees of shifting. Except for bP-Ni, the other metal electronic states distribute within the conduction bands of phosphorene. This leads to that electrons of metals are transferred to phosphorene and, correspondingly, the Fermi levels of phosphorene shift upward[21,41]. Thus, the phosphorene undergoes semiconductor-to-metal transition, due to upward shift of Fermi level, after AM, Ba and Tl decorations. For the bP-Ca, bP-Ca and bP-La systems, on the other hand, the lowest conduction bands of phosphorenes are pushed down relative to the other conduction bands due to the repulsive interaction of metal states. The spacings between the lowest and the second lowest conduction bands are of different degrees of increasing, especially for the AEM and La decorations cases[42]. When the Fermi levels shift upward and are located in the large spacings between the lowest and the second lowest conduction bands, the bP-Ca, bP-Ca and bP-La systems exhibit small indirect bandgaps. For the bP-Ni system, the states are mainly distributed in valence bands, leading to small amounts of electron transfer. Thus, the bP-Ni system remains the direct-bandgap-semiconductor property with band gap of 0.788 eV. The decrease of bandgap for the the bP-Ni system may be attributed to introduction of states near VBM. Additionally, the decoration of La atom causes the phosphorene to exhibit magnetism.

NH$_3$ gas molecule adsorption on bP-M. For the NH$_3$ molecules adsorption on bP-M systems, the various initial adsorption configurations are considered. The most stable adsorption configurations are obtained by comparing the adsorption energies after full geometry optimization. The most stable adsorption configurations are illustrated in Fig. 3, and their corresponding adsorption energies (E_{ads}) are listed in Table 1. All NH$_3$ molecules are stably adsorbed on bP-M systems with N atoms pointing toward the metal. The adsorption energies range from 0.238 to 1.305 eV for all the stable adsorbed cases, which are larger than that of 0.218 eV for adsorption on pristine phosphorene, indicating that the decoration of metal can improve the adsorption energy of phosphorene to NH$_3$ molecule. In addition, the charge transfer amounts (ΔQ) and adsorption distances ($D_{\text{P-Gas/M-Gas}}$) between NH$_3$ and metal decorated phosphorene are also summarized in Table 1. The largest adsorption energy and the largest charge transfer amount indicate the strongest adsorption of bP-Ni to NH$_3$.

Figure 4 shows the LDOS of NH$_3$ molecules adsorption on bP-M systems. The adsorptions of NH$_3$ molecules have little effect on the electronic structures of bP-Ms due to that the states of N and H atoms are far below the Fermi level. As shown in Fig. 4(j), the asymmetric LDOS distribution of bP-La adsorption system indicates that bP-La adsorption system is spin-polarized with magnetic moment of 0.990 μB, while the other bP-Ms adsorption systems have no spin polarization. The magnetic properties of bP-Ms with NH$_3$ adsorption are consistent with those without NH$_3$ adsorption, which are also corroborated by the band structures in Fig. S7, implying that NH$_3$ adsorption doesn't change magnetic property of bP-M adsorption systems.

The Fermi levels of the decorated substrates shift slightly due to the certain amount of electron transfer between the decorated substrates and NH$_3$ molecules. Except for bP-Sr, the conductive properties of the other bP-M system remain unchanged after NH$_3$ adsorptions. For example, the bP-AM (AM = Li, Na, K, Rb, Cs), bP-Ba and bP-Tl adsorption systems still remain metal properties, while the bP-Ca, bP-Ni and bP-La adsorption systems still remain semiconductor properties with the corresponding bandgaps of 0.045, 0.788, and 0.188 eV, respectively. For bP-Sr adsorption system, as shown in Figs 4(g) and S7(g), the Fermi level enters the second lowest conduction band of phosphorene, indicating that the bP-Sr undergoes semiconductor-to-metal transition after NH$_3$ adsorption. In addition, the overlap between the coupling peaks of N and H and the metal indicates strong hybridized interaction between them, which may be the cause that the metal decoration can improve the adsorption strength of phosphorene to NH$_3$ molecules. However, for the NH$_3$ molecule adsorption on the bP-Tl system, except for the N and H coupling peaks near −4 eV in Fig. 4(k), the N and H coupling peaks are not significantly associated with Tl LDOS, indicating the weak interaction between the NH$_3$ molecule and T1 atom.

NO gas molecules adsorption on bP-M. Three different adsorption configurations were modeled for NO adsorption on bP-M: the N-O bond is parallel to phosphorene plane and N-O bond is normal to phosphorus
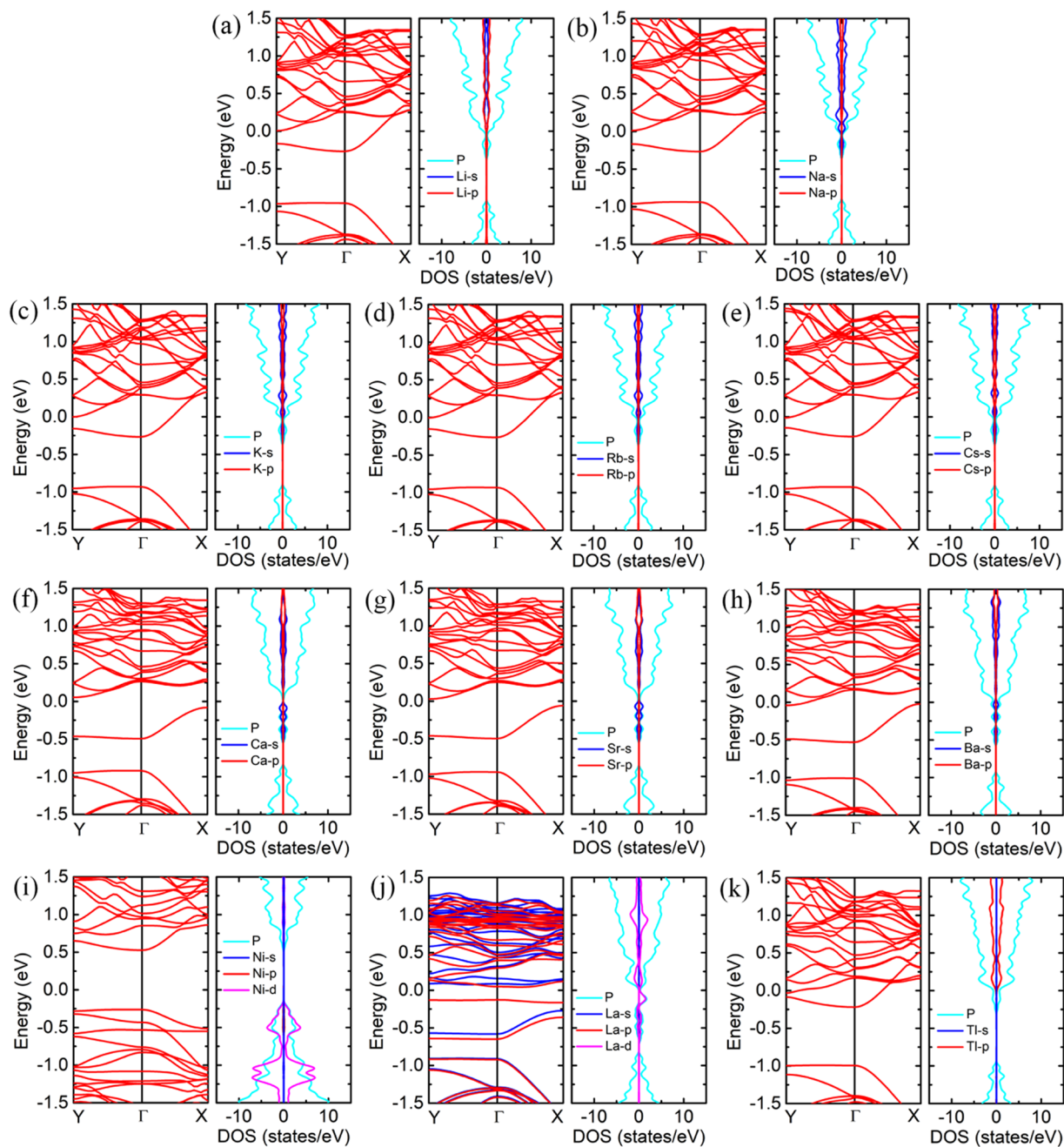
Figure 2. The band structures and PDOSs of (**a**) bP-Li, (**b**) bP-Na, (**c**) bP-K, (**d**) bP-Rb, (**e**) bP-Cs, (**f**) bP-Ca, (**g**) bP-Sr, (**h**) bP-Ba, (**i**) bP-Ni, (**j**) bP-La and (**k**) bP-Tl. The red and blue curves in the band structures represent the spin-up and spin-down bands, respectively. The cyan curves in PDOS represent the states for P atoms, and the blue, red and magenta curves represent the *s*-, *p*- and *d*-states for metal atoms.

plane with N or O pointing to metal atom. The results show that the NO molecule prefers the N atom to be close to the metal atom due to the larger adsorption energy, as shown in Fig. 5. The adsorption energies were calculated and summarized in Table 1. For the NO molecule adsorptions on bP-AM systems, the adsorption energies decrease with the increasing the atomic number of decoration atoms, that is, the largest adsorption energy of 0.831 eV for NO molecule on bP-Li and the smallest adsorption energy of 0.466 eV for NO molecule on bP-Cs. Similarly, the adsorption energies of NO molecules on bP-AEM are 1.538, 1.363 and 1.339 eV respectively, which decrease with increasing the atomic number of decoration atoms. On the other hand, from Table 1 we can see that the adsorption energies of NO molecule on bP-AEM are larger than those of NO molecule on bP-AM, indicating that the decoration of AEM are more effective than AM in improving the adsorption strength of phosphorene to NO molecules. The adsorption energies of NO on bP-Ni and bP-La are up to 2.121 and 2.475 eV, which are the largest adsorption energies. However, the NO molecule on bP-Tl has the smallest adsorption energy of 0.252 eV, which is even smaller than that on pristine phosphorene.
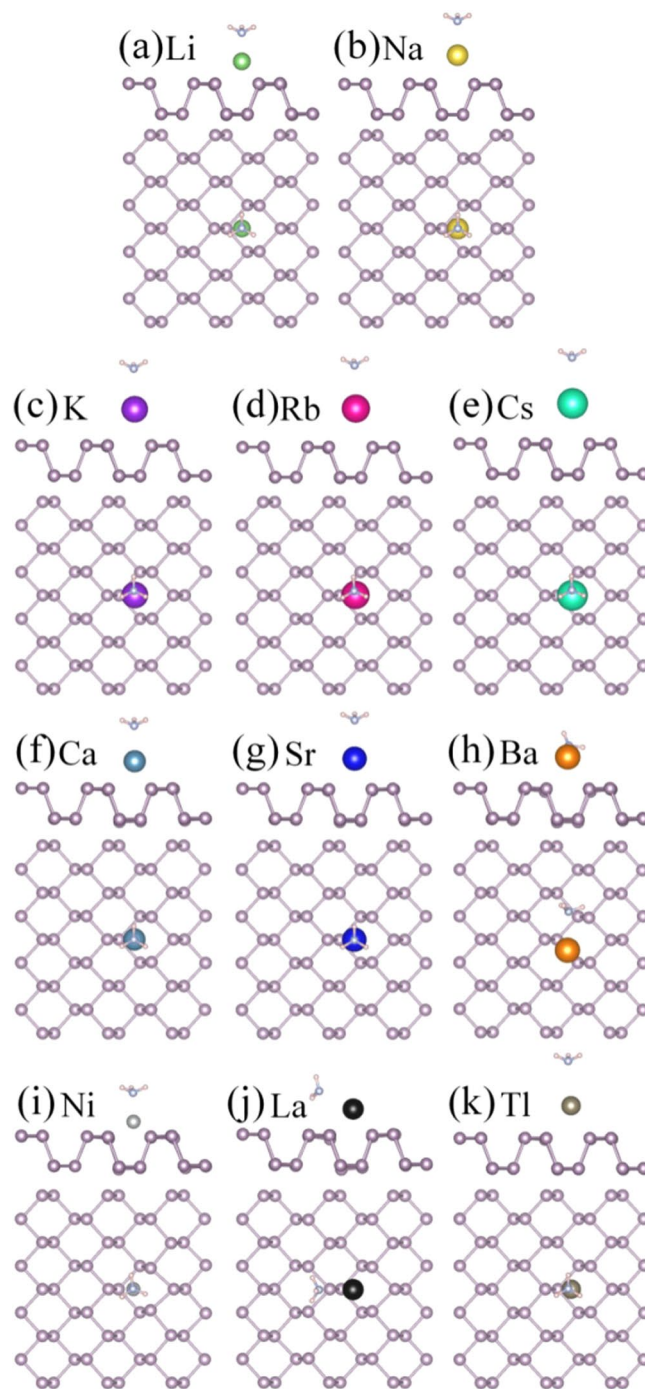
Figure 3. The optimized structures of NH_3 adsorption on bP-M (M = Li, Na, K, Rb, Cs, Ca, Sr, Ba, Ni, La, Tl). The green, gold, purple, red, cyan, dark cyan, blue, orange, light gray, black and gray balls represent Li, Na, K, Rb, Cs, Ca, Sr, Ba, Ni, La and Tl, respectively.

Figure 6 shows the LDOSs of NO molecule adsorptions on bP-M systems. The NO adsorption has large impact on the electronic properties of metal decorated phosphorene substrates. As shown in Fig. 6, all the LDOSs of adsorption systems exhibit asymmetric distribution, which means that spin polarizations present in all the bP-M systems. On the other words, except for bP-La system, the remaining bP-M systems undergo nonmagnetism-to-magnetism transition after NO adsorption. The magnetic moments of NO adsorbed bP-M systems are summarized in Table 1. Interestingly, except for the bP-La system, the adsorptions of NO molecules only introduce a significant spin-up peak in the bandgaps of all the other bP-M systems. The bP-La system has a large spin-up peak and a small spin-down peak, introduced by NO adsorption, in the bandgap.

From Fig. 6, we can see that the Fermi levels of the adsorption systems exhibit different degree of downward shifting due to the electrons transfer from the metal decorated phosphorene substrates to NO molecules.
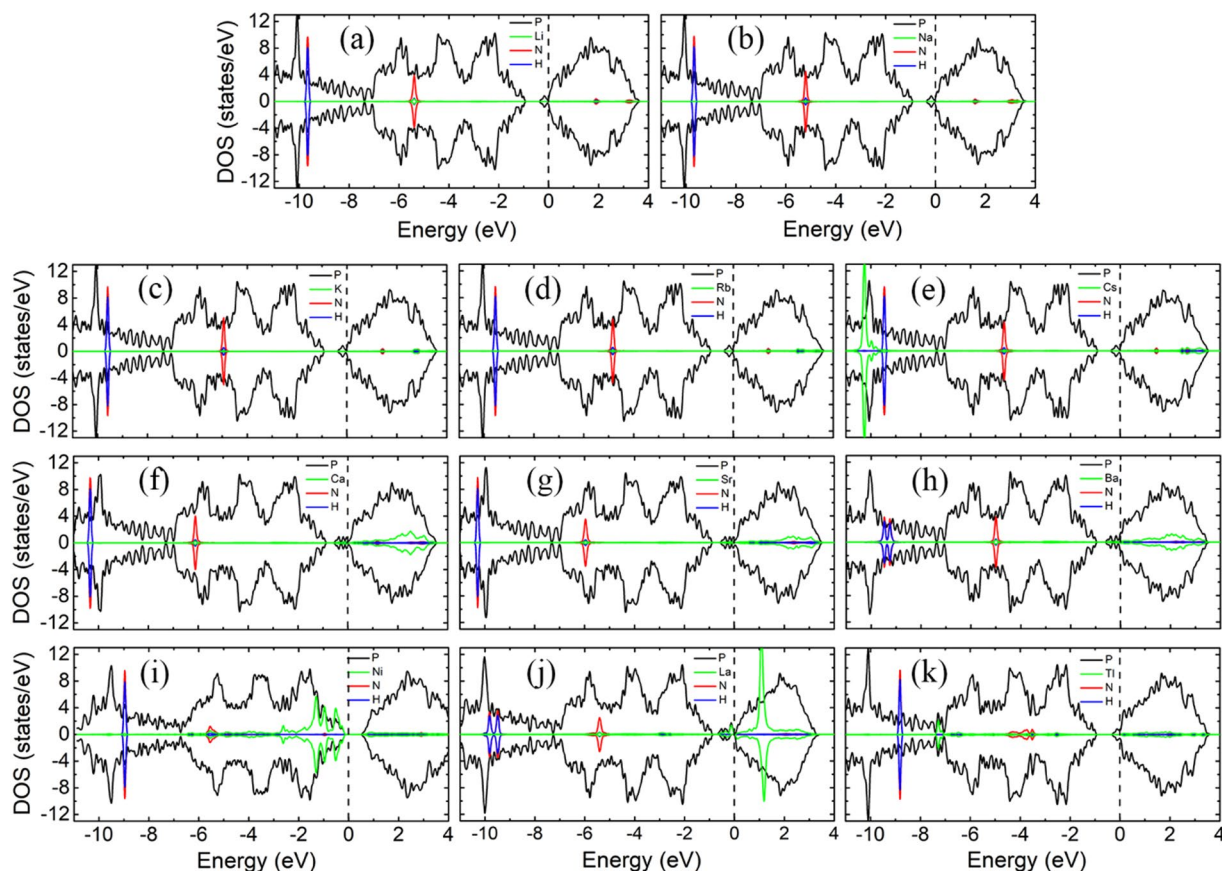
Figure 4. The LDOSs of NH_3 adsorption on bP-M (M = Li, Na, K, Rb, Cs, Ca, Sr, Ba, Ni, La, Tl). The black, green, red and blue curves represent the LDOS of P, metal, N and H, respectively. The Fermi level is set to zero.

Although the impurity states are introduced into the bandgap of the bP-Ni system, the adsorption of NO molecule doesn't change the conductive behavior of the bP-Ni system. That is, the bP-Ni system still remains the semiconductor property after NO adsorption. Furthermore, the band structure for NO adsorbed bP-Ni system in Fig. S8(i) is similar to that of the NO adsorbed on pristine phosphorene system, which indicates that metal decoration has little effect on the band structure of NO molecule adsorption on phosphorene. A slight upward shift of Fermi level for NO adsorbed on phosphorene is observed after Ni decoration, which may be ascribed to a small amount of electrons transfer from metal to phosphorene. The VBM of bP-Ni moves from Γ-point to Y-point after NO adsorption, and thus NO adsorbed bP-Ni system experiences direct-to-indirect transition with an indirect bandgap of 0.953 eV, which is larger than bandgap of 0.788 eV for without NO adsorption case. The increase of bandgap for the NO adsorbed bP-Ni system may be ascribed to charge transfer from bP-Ni substrate to NO molecule which results in the Ni states being lower the VBM of phosphorene. Except for the bP-Ni adsorption systems, the LDOSs of all the other bP-M adsorption systems at Fermi level are non-zero, implying that all the other bP-M adsorption systems are of metallic conductivities, which can also be demonstrated by Fig. S8. As compared with the bP-M systems without gas molecule adsorptions, the bP-Ca, bP-Sr, and bP-La adsorption systems experience semiconductor-to-metal transition after NO molecule adsorption, while the conductive properties of other bP-M adsorption systems remain unchanged. Furthermore, the lowest conduction bands of bP-M adsorption systems, especially for those of bP-AEM ones, are pushed up. The separations between the lowest and the second lowest conduction bands decrease, which may be due to that the repulsive interactions between the NO states above Fermi levels and the lowest conduction band of phosphorene are weakened by the interactions of NO molecule with metal atoms[43].

As mentioned above, except for Tl decoration case, all the metal decoration can increase the adsorption energies of NO adsorption on phosphorene, and thus improve the adsorption of phosphorene to NO molecules. For the bP-AM adsorption system, the states of AM atoms distribute mainly in conduction bands as mentioned before, and thus the peaks, near VBM and in the conduction bands, from N and O atomic states hybridized with those of AM atoms. For the bP-AEM adsorption system, the spin-up states in bandgap from NO molecules overlap significantly with those from AEM atoms, which account for the larger adsorption energies of NO adsorbed bP-AEM systems. For the LDOSs of NO adsorbed bP-Ni as depicted in Fig. 6(i), the energy positions of NO LDOS peaks are almost unchanged as compared with the LDOSs of NO adsorbed pristine phosphorene except for slight shift due to electrons transferring between Ni and phosphorene. However, the hybridization of Ni LDOS peaks with NO LDOS peaks can be seen clearly in Fig. 6(i). Similarly, the strong hybridization of La LDOS peaks
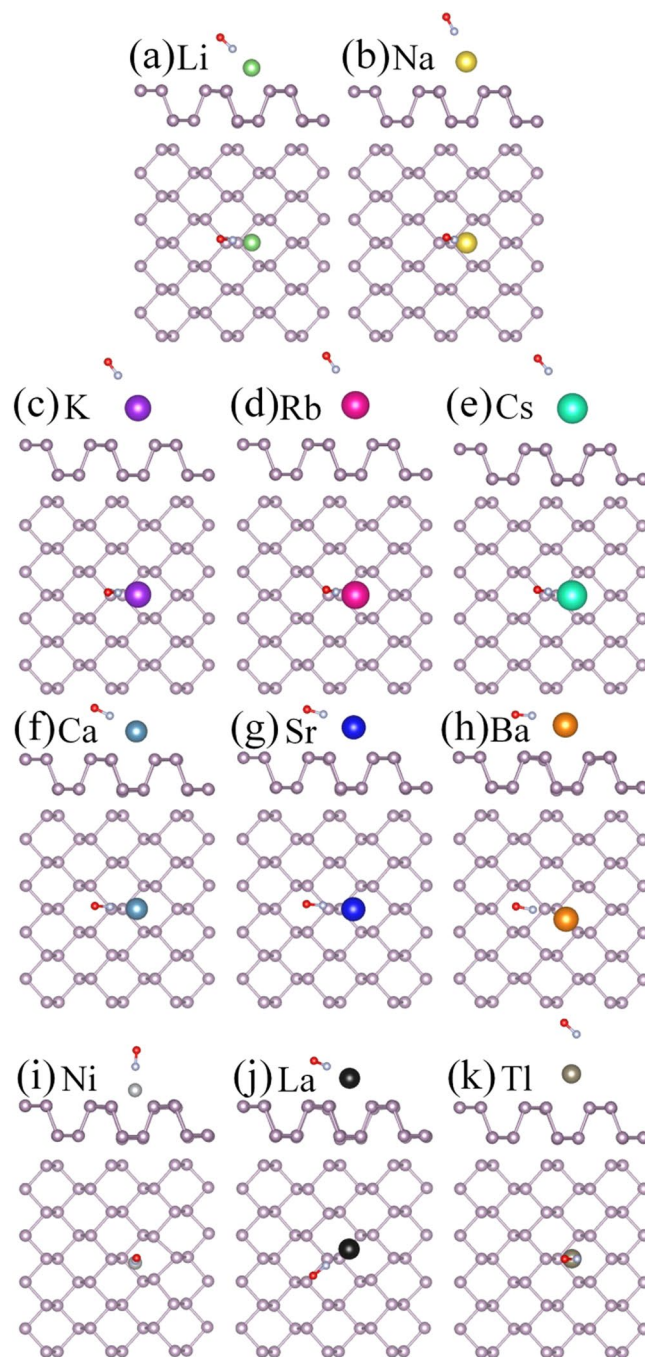
Figure 5. The optimized structures of NO adsorption on bP-M (M = Li, Na, K, Rb, Cs, Ca, Sr, Ba, Ni, La, Tl). The green, gold, purple, red, cyan, dark cyan, blue, orange, light gray, black and gray balls represent Li, Na, K, Rb, Cs, Ca, Sr, Ba, Ni, La and Tl, respectively.

with NO LDOS peaks, especially the peaks near Fermi level, can be found in Fig. 6(j), which may be the cause of the largest adsorption energy.

NO$_2$ gas molecules adsorption on bP-M. Various initial adsorption configurations are considered and the most stable adsorption configurations are picked out, by comparing the adsorption energies of various initial configurations, as illustrated in Fig. 7. The adsorption energies for the most stable configurations are list in Table 1. The NO$_2$ molecule is adsorbed on the bP-Ni system with the bond angle away from Ni atom, while the remaining NO$_2$ molecules are stably adsorbed on the metal decorated substrates with the bond angles toward metal atoms. Similar to NO molecules, the adsorption energies of NO$_2$ molecules on bP-AM and bP-AEM systems decrease with increasing the atomic number of decoration atoms, and the adsorption energies of NO$_2$ on bP-AEM are larger than those on bP-AM (see Fig. S6 and Table 1). For transition metal Ni and La decorated
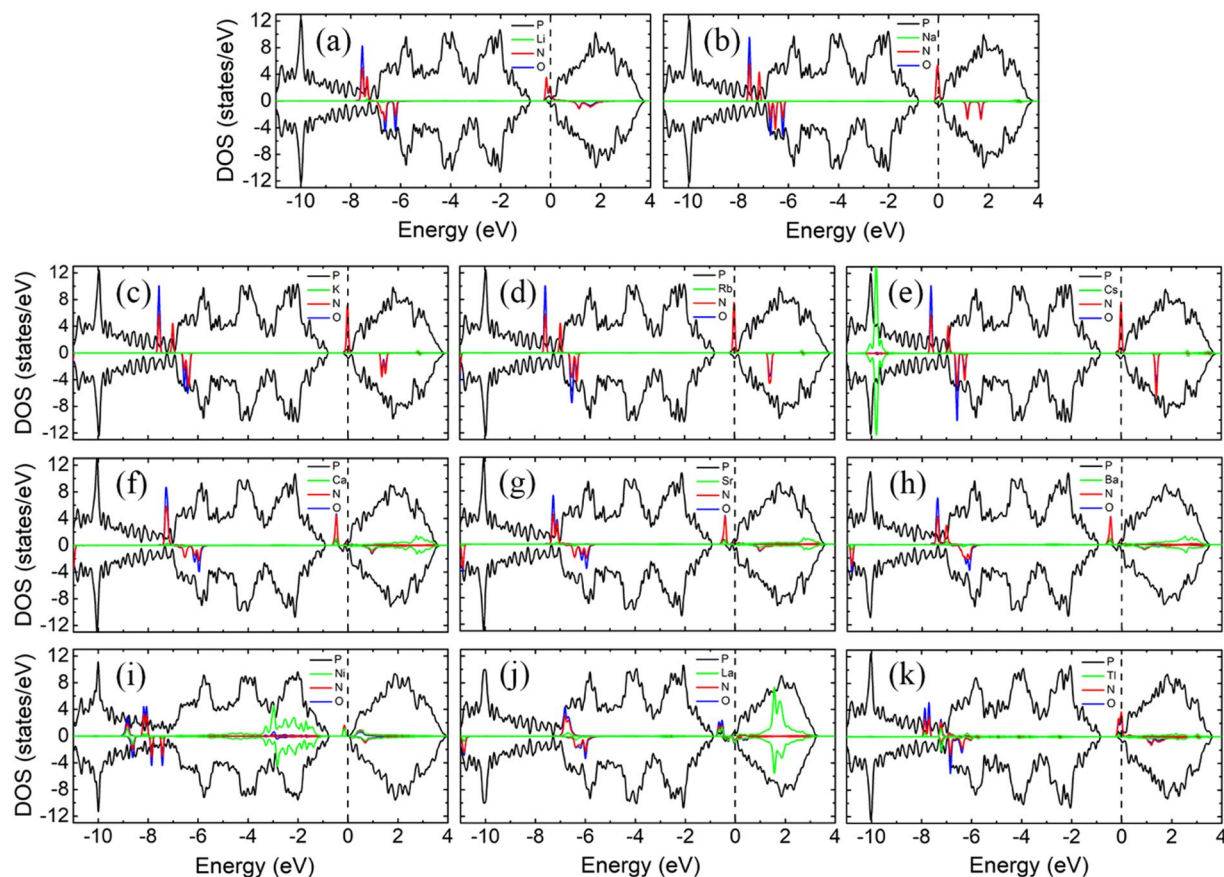
Figure 6. The LDOSs of NO adsorption on bP-M (M = Li, Na, K, Rb, Cs, Ca, Sr, Ba, Ni, La, Tl). The black, green, red and blue curves represent the LDOS of P, metal, N and O, respectively. The Fermi level is set to zero.

phosphorene cases, the corresponding NO-molecule adsorption energies are 1.818 and 3.734 eV, respectively. The adsorption energy of NO_2 molecule on bP-La is the largest among all adsorption energies. The adsorption energy of NO_2 molecule on bP-Tl is only 1.773 eV.

To better understand the effects of NO_2 molecules on the bP-M systems, the LDOSs of NO_2 molecule adsorbed bP-M systems are shown in Fig. 8. The LDOSs of bP-K, bP-Rb, bP-Cs and bP-Ni adsorption systems exhibit obvious asymmetry distribution, indicating that bP-K, bP-Rb, bP-Cs and bP-Ni are spin polarized with magnetic moment of 0.166, 0.192, 0.240 and 1.000 μB, respectively, as given in Table 1. The spin polarized character of bP-K, bP-Rb, bP-Cs and bP-Ni adsorption systems can also be corroborated by the band structures in Fig. S9. All the other NO_2 adsorbed bP-M systems exhibit non-spin polarized characters. Especially for bP-La system, which is spin polarized before gas molecule adsorption, it exhibits symmetric distributed LDOS after NO_2 adsorption, indicating that bP-La adsorption system is non-spin polarized with zero magnetic moments (see Table 1). Disappearance of the magnetism for bP-La adsorption system may be attributed that the spin polarization of the substrate is inhibited by the adsorption of NO_2. As compared with bP-Ms without gas molecule adsorptions case, the bP-K, bP-Rb, bP-Cs and bP-Ni systems experience nonmagnetism-to-magnetism transition, while the bP-La system experiences magnetism-to-nonmagnetism transition, after NO_2 adsorption.

From Table 1, we can see that the electrons transfer from bP-M substrates to NO_2 molecules for all the NO_2 adsorbed bP-M systems, which implies that the Fermi levels of all the bP-M systems shift down after NO_2 molecule adsorptions. For bP-K, bP-Rb and bP-Cs adsorption systems, the N and O atoms introduce a spin-up peak in the bandgap and a spin-down peak at the CBM. The Fermi levels of bP-K, bP-Rb and bP-Cs shift to the CBM and cross through the spin-down states of N and O atoms, leading to the metal properties. For bP-Li and bP-Na systems, the N and O atoms introduce the symmetric states near VBM and CBM for bP-Li and bP-Na adsorption systems, respectively. The Fermi levels of bP-Li and bP-Na systems shift downward into the bandgaps of phosphorene after NO_2 molecule adsorptions, indicating that the NO_2 adsorbed bP-Li and bP-Na systems are semiconductors. The bandgaps of NO_2 adsorbed bP-Li and bP-Na are 0.921 and 0.902 eV, respectively, which are slightly larger than that of pristine phosphorene. This may be ascribed to decrease of repulsive interaction between the facing lone pair electrons at channel due to the wider channel[42]. For bP-AEM systems, as shown in Figs 8(f–h) and S9(f–h), the separations between the lowest and the second lowest conduction bands significantly decrease due to that the adsorptions of NO_2 molecules weaken the repulsive interaction between the Ni atom states and the lowest conduction band of phosphorene[42]. This leads to the lowest conduction bands shifting upward, and the Fermi levels cross through the lowest conduction bands. Thus, the NO_2 adsorbed bP-Ca, bP-Sr and bP-Ba systems exhibit the metal properties. As shown in Fig. 8(i), the adsorption of NO_2 weakens the interaction between Ni
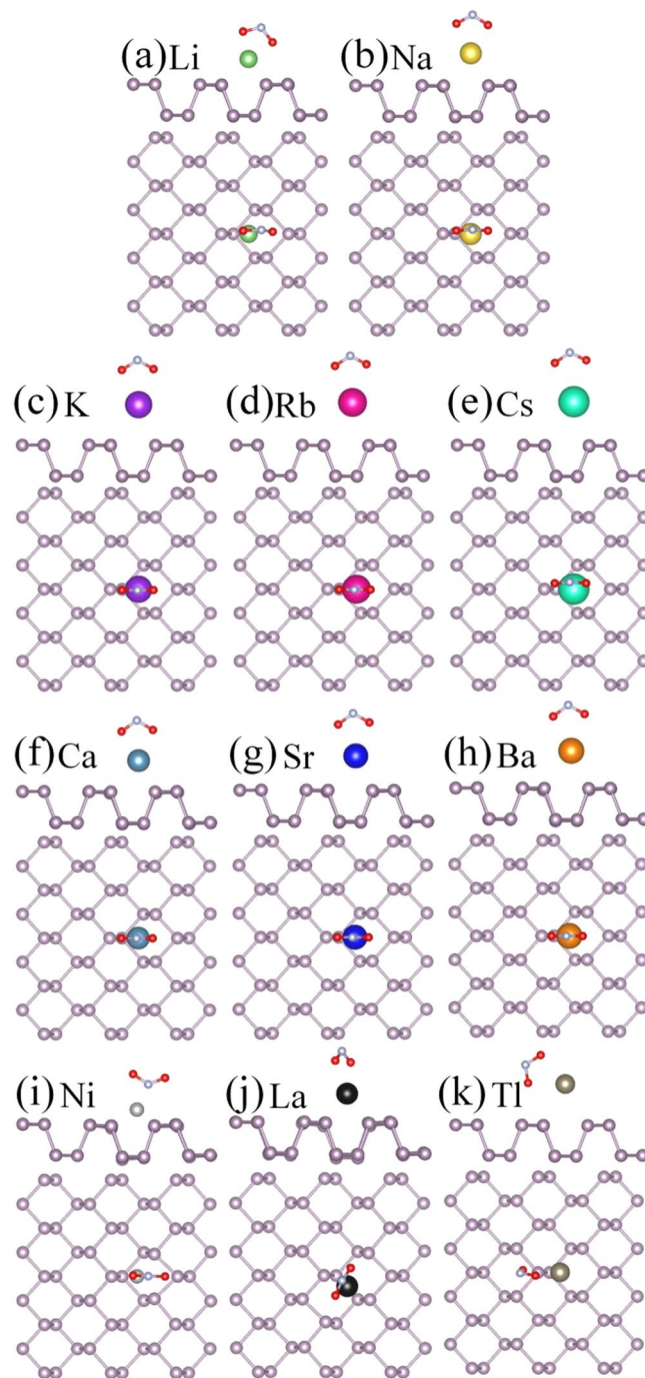
Figure 7. The optimized structures of NO$_2$ adsorption on bP-M (M = Li, Na, K, Rb, Cs, Ca, Sr, Ba, Ni, La, Tl). The green, gold, purple, red, cyan, dark cyan, bule, orange, light gray, black and gray balls represent Li, Na, K, Rb, Cs, Ca, Sr, Ba, Ni, La and Tl, respectively.

atom and the phosphorene, and thus the Ni atom states are away from VBM of phosphorene. This leads to the band of bP-Ni shifting slightly downward. Moreover, the VBM shifts from the Γ- to Y-point, which makes the bP-Ni adsorption system become into an indirect bandgap semiconductor. As shown in Fig. 8(j), compared with before NO$_2$ adsorption, the impurity band of bP-La near the Fermi level disappears after NO$_2$ adsorption. Thus, bP-La remains the small indirect-bandgap-semiconductor properties. In Fig. 8(k), similar to bP-Li and bP-Na systems, the adsorption of NO$_2$ molecules causes the Fermi level to shift from the conduction band significantly downward into the bandgap. Thus, bP-Tl exhibits semiconductor properties after NO$_2$ adsorption, and the corresponding bandgap is 0.924 eV. Therefore, after NO$_2$ adsorption, the bP-Li, bP-Na, and bP-Tl systems undergo metal-to-semiconductor transition, while the bP-Ca and bP-Sr systems undergo semiconductor-to-metal transition. Additionally, the bP-Ni system remains semiconductor property, but it undergoes direct-to-indirect transition after NO$_2$ adsorption.
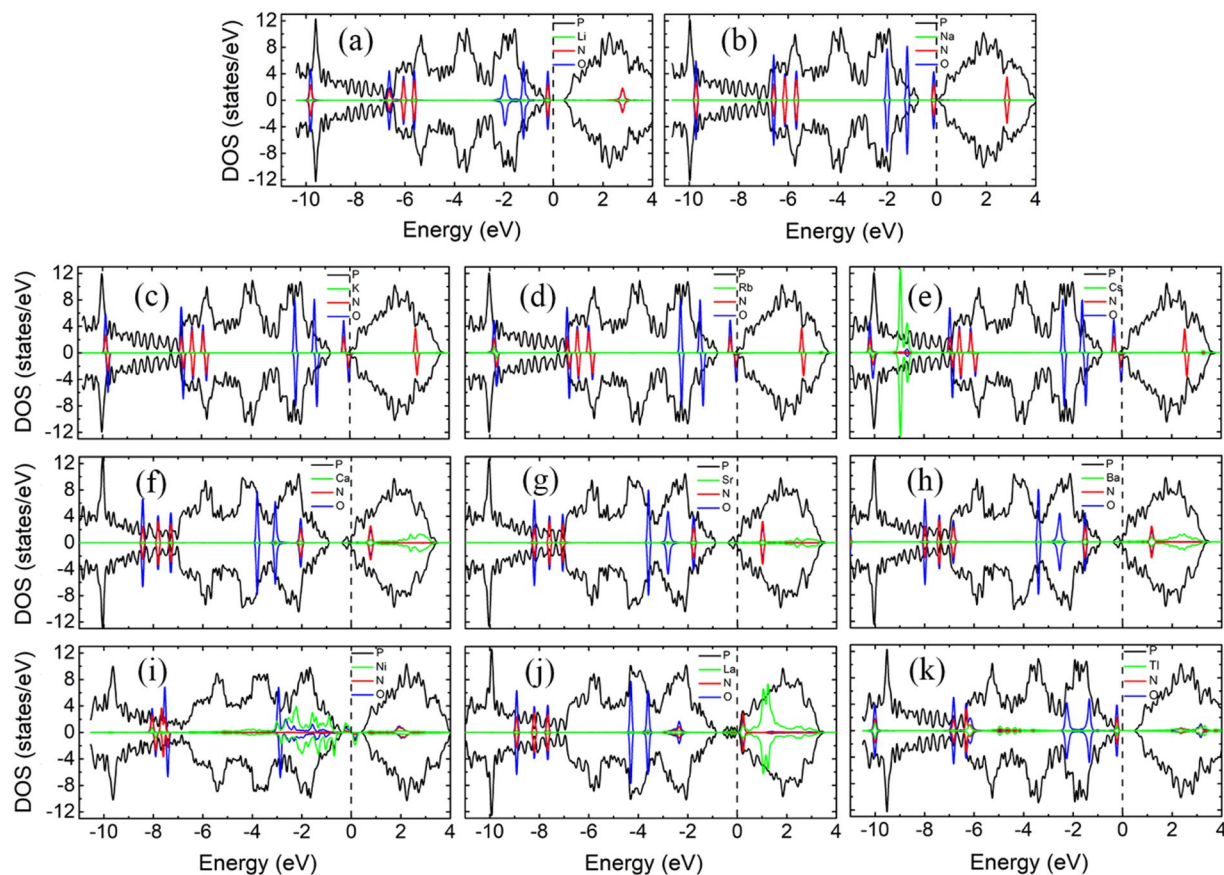
Figure 8. The LDOSs of NO_2 adsorption on bP-M (M = Li, Na, K, Rb, Cs, Ca, Sr, Ba, Ni, La, Tl). The black, green, red and blue curves represent the LDOS of P, metal, N and O, respectively. The Fermi level is set to zero.

The coupling peaks between the NO_2 molecules and metals of NO_2 adsorbed bP-AEM systems are more widely distributed, especially in the conduction band, than those of NO_2 adsorbed bP-AM systems, which may account for that the AEM decoration is more effective in improving the adsorption strength of NO_2 gas molecules on phosphorene. For bP-La adsorption system, the strong coupling peaks between the NO_2 molecules and metal are observed around Fermi level, indicating a strong electronic interaction of the NO_2 gas molecule with metal and thus the largest adsorption energy as shown in Table 1.

Conclusions

In conclusion, the nitrogen-based gas molecules (NH_3, NO, NO_2) adsorption on metal (Li, Na, K, Rb, Cs, Ca, Sr, Ba, Ni, La, Tl) decorated phosphorene has been studied by using first-principles calculation based on DFT. Except for NO adsorption on bP-Tl, all metal decorations can improve the adsorption strength of phosphorene to nitrogen-based gas molecules. For NH_3 and NO, the adsorption energies follow an energy order of E_{ads} (bP-TM) > E_{ads} (bP-AEM) > E_{ads} (bP-AM) > E_{ads} (bP-Tl), while the NO_2 follow an energy order of E_{ads} (bP-La) > E_{ads} (bP-AEM) > E_{ads} (bP-AM). The largest energies of NH_3, NO and NO_2 adsorbed bP-M are 1.305, 2.475 and 3.734 eV, respectively. In addition, the band structures and LDOSs show that NH_3 has little effect on electronic and magnetic properties of bP-M substrates, while the adsorptions of NO and NO_2 make an interesting change in electronic and magnetic properties of bP-M. For example, except for bP-La, the metal decorated substrates exhibit nonmagnetism-to-magnetism after NO adsorption, and the bP-Ca, bP-Sr and bP-La undergo semiconductor-to-metal transition. Similarly, the magnetic states of some decorated substrates (bP-K, bP-Rb, bP-Cs, bP-Ni, bP-La) change after NO_2 adsorption, and especially the spin polarization for bP-La systems disappear after NO_2 adsorption. Furthermore, the bP-Li, bP-Na and bP-Tl experience metal-to-semiconductor transition, while bP-Ca and bP-Sr undergo semiconductor-to-metal transition due to large electron transfer amounts between NO_2 and decorated substrates. These results indicate that the metal decoration can be used for the removal and detection of nitrogen-based gas.

References

1. Khan, Md. S., Srivastava, A. & Pandey, R. Electronic properties of a pristine and NH_3/NO_2 adsorbed buckled arsenene monolayer. *RSC Adv.* **6**, 72634–72642 (2016).
2. Khan, Md. A. H., Rao, M. V. & Li, Q. Recent advances in electrochemical sensors for detecting toxic gases: NO_2, SO_2 and H_2S. *Sensors* **19**, 905 (2019).
3. Arabieh, M. & Azar, Y. T. In silico insight into ammonia adsorption on pristine and X-doped phosphorene (X = B, C, N, O, Si, and Ni). *Appl. Surf. Sci.* **396**, 1411–1419 (2017).

4. Genc, S., Zadeoglulari, Z., Fuss, S. H. & Genc, K. The adverse effects of air pollution on the nervous system. *J. Toxicol.* **2012**, 782462 (2012).
5. Lee, S. W., Lee, W., Hong, Y., Lee, G. & Yoon, D. S. Recent advances in carbon material-based NO₂ gas sensors. *Sensor. Actuator. B Chem.* **255**, 1788–1804 (2018).
6. Endres, H.-E. *et al*. A thin-film SnO₂ sensor system for simultaneous detection of CO and NO₂ with neural signal evaluation. *Sensor. Actuator. B Chem.* **36**, 353–357 (1996).
7. Tomchenko, A. A., Harmer, G. P., Marquis, B. T. & Allen, J. W. Semiconducting metal oxide sensor array for the selective detection of combustion gases. *Sensor. Actuator. B Chem.* **93**, 126–134 (2003).
8. Seiyama, T., Kato, A., Fujiishi, K. & Nagatani, M. A new detector for gaseous components using semiconductive thin films. *Anal. Chem.* **34**, 1502–1503 (1962).
9. Arafat, M. M., Dinan, B., Akbar, S. A. & Haseeb, A. S. M. A. Gas sensors based on one dimensional nanostructured metal-oxides: A Review. *Sensors* **12**, 7207–7258 (2012).
10. Capone, S. *et al*. Solid state gas sensors: State of the art and future activities. *Optoelectronics Adv. Mater.* **5**, 1335–1348 (2003).
11. Novoselov, K. S. *et al*. Electric field effect in atomically thin carbon films. *Science* **306**, 666–669 (2004).
12. Geim, A. K. & Novoselov, K. S. The rise of graphene. *Nat. Mater.* **6**, 183–191 (2007).
13. Ratinac, K. R., Yang, W., Ringer, S. P. & Braet, F. Toward ubiquitous environmental gas sensors-capitalizing on the promise of graphene. *Environ. Sci. Technol.* **44**, 1167–1176 (2010).
14. Rumyantsev, S., Liu, G., Shur, M. S., Potyrailo, R. A. & Balandin, A. A. Selective gas sensing with a single pristine graphene transistor. *Nano Lett.* **12**, 2294–229 (2012).
15. Potyrailo, R. A., Surman, C., Nagraj, N. & Burns, A. Materials and transducers toward selective wireless gas sensing. *Chem. Rev.* **111**, 7315–7354 (2011).
16. Schedin, F. *et al*. Detection of individual gas molecules adsorbed on graphene. *Nat. Mater.* **6**, 652–655 (2007).
17. Leenaerts, O., Partoens, B. & Peeters, F. M. Adsorption of H₂O, NH₃, CO, NO₂, and NO on graphene: A first-principles study. *Phys. Rev. B* **77**, 125416 (2008).
18. Dai, J., Yuan, J. & Giannozzi, P. Gas adsorption on graphene doped with B, N, Al, and S: A theoretical study. *Appl. Phys. Lett.* **95**, 232105 (2009).
19. Ma, L., Zhang, J. M., Xu, K. W. & Ji, V. A first-principles study on gas sensing properties of graphene and Pd-doped graphene. *Appl. Surf. Sci.* **343**, 121–127 (2015).
20. Wu, L. *et al*. Lanthanide-coordinated black phosphorus. *Small* **14**, 1801405 (2018).
21. Kulish, V. V., Malyi, O. I., Persson, C. & Wu, P. Adsorption of metal adatoms on single-layer phosphorene. *Phys. Chem. Chem. Phys.* **17**, 992–1000 (2015).
22. Cai, Y., Ke, Q., Zhang, G. & Zhang, Y. Energetics, charge transfer, and magnetism of small molecules physisorbed on phosphorene. *J. Phys. Chem. C* **119**, 3102–3110 (2015).
23. Kou, L., Frauenheim, T. & Chen, C. Phosphorene as a superior gas sensor: Selective adsorption and distinct I-V response. *J. Phys. Chem. Lett.* **5**, 2675–2681 (2014).
24. Yang, B. C. *et al*. Te-Doped Black Phosphorus Field-Effect Transistors. *Adv. Mater.* **28**, 9408–9415 (2016).
25. Cui, S. *et al*. Ultrahigh sensitivity and layer-dependent sensing performance of phosphorene-based gas sensors. *Nat. Commun.* **6**, 8632 (2015).
26. Abbas, A. N. *et al*. Black phosphorus gas sensors. *ACS Nano* **9**, 5618–5624 (2015).
27. Li, W., Yang, Y., Zhang, G. & Zhang, Y. Ultrafast and directional diffusion of lithium in phosphorene for high-performance lithium-ion battery. *Nano Lett.* **15**, 1691–1697 (2015).
28. Zhao, S., Kang, W. & Xue, J. The potential application of phosphorene as an anode material in Li-ion batteries. *J. Mater. Chem. A* **2**, 19046–19052 (2014).
29. Ramireddy, T. *et al*. Phosphorus-carbon nanocomposite anodes for lithium-ion and sodium-ion batteries. *J. Mater. Chem. A* **3**, 5572–5584 (2015).
30. Yao, Q. *et al*. Theoretical prediction of phosphorene and nanoribbons as fast-charging Li ion battery anode materials. *J. Phys. Chem. C* **119**, 6923–6928 (2015).
31. Yu, Z., Wan, N., Lei, S. & Yu, H. Enhanced hydrogen storage by using lithium decoration on phosphorene. *J. Appl. Phys.* **120**, 024305 (2016).
32. Li, Q., Wan, X. G., Duan, C. & Kuo, J. Theoretical prediction of hydrogen storage on Li-decorated monolayer black phosphorus. *J. Phys. D: Appl. Phys.* **47**, 465302 (2014).
33. Kuang, A. *et al*. Acidic gases (CO₂, NO₂ and SO₂) capture and dissociation on metal decorated phosphorene. *Appl. Surf. Sci.* **410**, 505–512 (2017).
34. Kuang, A. *et al*. Adsorption and decomposition of metal decorated phosphorene toward H₂S, HCN and NH₃ molecules. *Appl. Surf. Sci.* **473**, 242–250 (2019).
35. Lei, S. Y. *et al*. CO adsorption on metal-decorated phosphorene. *ACS Omega* **3**, 3957–3965 (2018).
36. Kresse, G. & Furthmüller, J. Efficient iterative schemes for ab initio total-energy calculations using a plane-wave basis set. *Phys. Rev. B* **54**, 11169–11186 (1996).
37. Kresse, G. & Furthmüller, J. Efficiency of ab-initio total energy calculations for metals and semiconductors using a plane-wave basis set. *Comput. Mater. Sci.* **6**, 15–50 (1996).
38. Perdew, J. P., Burke, K. & Ernzerhof, M. Generalized gradient approximation made simple. *Phys. Rev. Lett.* **77**, 3865–3868 (1996).
39. Grimme, S. Semiempirical GGA-type density functional constructed with a long-range dispersion correction. *J. Comput. Chem.* **27**, 1787–1799 (2006).
40. Li, X. *et al*. Structures, stabilities, and electronic properties of defects in monolayer black phosphorus. *Sci. Rep.* **5**, 10848 (2015).
41. Suvansinpan, N. *et al*. Substitutionally doped phosphorene: Electronic properties and gas sensing. *Nanotechnology* **27**, 065708 (2016).
42. Ienco, A., Manca, G., Peruzzini, M. & Mealli, C. Modelling strategies for the covalent functionalization of 2D phosphorene. *Dalton Trans.* **47**, 17243–17256 (2018).
43. Lei, S. *et al*. Enhancing the ambient stability of few-layer black phosphorus by surface modification. *RSC Adv.* **8**, 14676–14683 (2018).

Acknowledgements

Author Contributions

S. Lei gave the idea. S. Lei, R. Gao and X. Sun carried out first-principles calculation. S. Lei and X. Sun wrote the main manuscript text. S. Lei, X. Sun and S. Guo prepared all figures and tables in the manuscript. R. Gao, H. Yu, N. Wan, F. Xu and J. Chen assisted S. Lei to analyze the results.

Additional Information

Supplementary information accompanies this paper at https://doi.org/10.1038/s41598-019-48953-0.

Competing Interests: The authors declare no competing interests.

Publisher's note: Springer Nature remains neutral with regard to jurisdictional claims in published maps and institutional affiliations.